

# Electrostatically Driven Protein Aggregation: $\beta$ -Lactoglobulin at Low Ionic Strength

Pinaki R. Majhi,<sup>†</sup> Reddy R. Ganta, Ram P. Vanam, Emek Seyrek, Katie Giger, and Paul L. Dubin<sup>\*,‡</sup>

Department of Chemistry, Indiana University-Purdue University at Indianapolis,  
402 North Blackford Street, Indianapolis, Indiana 46202

Received December 31, 2005. In Final Form: July 28, 2006

The aggregation of  $\beta$ -lactoglobulin (BLG) at ambient temperature was studied using turbidimetry and dynamic light scattering in the range  $3.8 < \text{pH} < 5.2$  in 0.0045 M NaCl, and in the ionic strength range 0.0045–0.5 M at fixed  $\text{pH} = 5.0$ . The initial rate of aggregation, taken as the initial slope of turbidity vs time,  $(d\tau/dt)_0$ , indicated maximum aggregation near  $\text{pH} 4.6$  (below the isoelectric point of 5.2), but the dependence of the initial rate of aggregation on  $\text{pH}$  was highly asymmetric. At  $\text{pH} 5.0$ ,  $(d\tau/dt)_0$  strongly increased with a decrease in ionic strength  $I$  from 0.1 to 0.0045 M and was found to be nearly linear with  $1/I$ . DLS measurements revealed an increase in particle size with time, with the appearance of bimodal distributions in which the fast and slow modes corresponded, respectively, to a BLG dimer and to larger aggregates in the 100–800 nm range. At conditions of slower aggregation, DLS revealed the consumption of dimers to form higher order aggregates with no intermediate species. Computer modeling (Delphi) was used to visualize the electrostatic potential around the dimer to elucidate the  $\text{pH}$  and ionic strength dependence of the initial aggregation rates. The aggregation process appears to comprise an initial fast consumption of the dimer, whose dependence on  $\text{pH}$  and  $I$  arises from the interaction of the positive and negative domains of interacting dimers, followed by the slow formation of much larger aggregates with relatively little sensitivity to  $\text{pH}$  and  $I$ . The open-ended nature of BLG aggregation is thought to arise from the asymmetry of the dimer charge distribution.

## Introduction

Protein aggregation is an inevitable consequence of cellular existence and is an important factor in a variety of pharmaceutical processes. Almost all proteins tend to aggregate, but in different ways and to different extents under different conditions. Understanding protein aggregation *in vivo* is important to obtain insight into a range of diseases from sickle-cell anemia<sup>1</sup> to Alzheimer's disease.<sup>2</sup> From an industrial point of view, protein aggregation is relevant to a variety of biotechnological processes and pharmaceutical applications including the formation and renaturation of inclusion bodies and the formulation and storage stability of protein drugs. The growing number of protein drugs as well as the recognition of the importance of protein aggregation in critical disease states thus motivates intense research on both the equilibrium and dynamic aspects of protein aggregation. Included in this effort is the need to understand the forces that drive protein–protein association and to regulate these forces.

The terms “aggregation” and “association” are often used interchangeably in the protein literature. Without attempting to resolve this ambiguity, one can clearly distinguish between reversible and irreversible phenomena. The former usually starts from the native state, which under certain conditions salts out at protein concentrations exceeding the solubility limit, or undergoes “isoelectric precipitation” when the net protein charge is near zero. Irreversible aggregation, on the other hand, occurs when misfolded and unassembled proteins inappropriately expose

hydrophobic surfaces that are normally buried in the protein's interior, or takes place at the interface of subunits on exposure to extremes of  $\text{pH}$  or temperature. The second type of phenomenon, irreversible aggregation, is almost impossible to predict on the basis of protein structure.

The aggregation of  $\beta$ -lactoglobulin (BLG) has been studied intensively, the results including a range of conditions that encompass the formation of well-defined multimers, higher order aggregation, phase separation, and gelation. Much of the literature on the parameters affecting BLG aggregation is inextricably tied in with temperature effects. To a considerable degree, this work is motivated by the consequences for the food industry of high-temperature aggregation of whey protein, in which BLG is a major component.<sup>3</sup> While the studies reported here are under non-denaturing conditions, the effects of  $\text{pH}$  and ionic strength central to the current work have also been noted at high temperatures and are therefore worth mentioning. Irreversible protein aggregation often occurs upon heating and has been particularly studied with BLG, since this dominates the overall aggregation and gelation behavior of whey protein preparations, which leads to fouling of heat exchangers in dairy processing.<sup>4</sup> The true physiological function of BLG is still an intriguing question; however, it has been implicated in the transport of retinol<sup>5</sup> and in the *in vitro* binding of milk fatty acids and a number of other small hydrophobic molecules. BLG in its natural state consists of two main genetic variants, “A” and “B”, and self-association is more pronounced for BLG-A than for BLG-B.<sup>6–7</sup> Existing mainly as a noncovalently linked dimer at room

\* To whom correspondence should be addressed. E-mail: dubin@chem.umass.edu.

<sup>†</sup> Present address: Department of Pharmaceutical Chemistry, University of California, San Francisco, 513 Parnassus Ave., Campus Box 0446, San Francisco, CA 94143.

<sup>‡</sup> Current address: Department of Chemistry, University of Massachusetts, Amherst, MA 01003.

(1) Merlini, G. B.; Vittorio, A.; Palladini, G.; Obici, L.; Casarini, S.; Perfetti, V. Protein aggregation. *Clin. Chem. Lab. Med.* **2001**, *39*, 1065.

(2) Iversen, L. L.; Mortishire-Smith, R. J.; *Biochem. J.* **1995**, *311*, 1.

(3) Ju, Z. Y.; Kilara, A. *J. Agric. Food Chem.* **1998**, *46*, 3604

(4) de Jong, P. *Trends Food Sci. Technol.* **1997**, *8*, 401.

(5) Papiz, M. Z.; Sawyer, L.; Eliopoulos, E. E.; North, A. C.; Findlay, J. B.; Sivaprasadarao, R.; Jones, T. A.; Newcomer, M. E.; Kraulis, P. J. *Nature* **1986**, *24*, 383.

(6) Gottschalk, M.; Nilsson, H. *Protein Sci.* **2003**, *12*, 2404 and references therein.

(7) Timasheff, S. N.; Townend, Robert. *J. Am. Chem. Soc.* **1958**, *80*, 4433.

temperature and physiological conditions,<sup>8</sup> BLG on heating dissociates into monomers, which denature irreversibly<sup>9</sup> and aggregate<sup>10,11</sup> on increasing the temperature to about 50 °C. Covalent bond formation during heat-induced aggregation involves partial unfolding of monomers, leading to the exposure of previously buried inner hydrophobic groups and the free thiol group at C121. The occurrence of thiol/disulfide exchange reactions and their involvement in heat-induced aggregation and gelation have been demonstrated in a number of studies.<sup>12–17</sup> The mechanism of heat-induced aggregation is also sensitive to pH: In the early stages of aggregation, it was reported that disulfide-linked aggregates form on heating at pH 6.7 but not at pH 4.9.<sup>18</sup> The overall implication is that heat-induced aggregation involves partial denaturation.

Despite its instability at high temperatures, BLG has been used as a molecular weight standard, largely because of its abundance, ease of purification, and stability as a dimer at room temperature and physiological conditions.<sup>19</sup> Bovine BLG has been the subject of many physicochemical studies. The large amount of literature accumulated over the past 60 years shows that BLG has been studied by essentially every biochemical technique. For example, measurements by osmotic pressure,<sup>20</sup> X-ray diffraction,<sup>21</sup> sedimentation and diffusion<sup>22</sup> and light scattering<sup>23</sup> all yield a value for the dimer molecular weight close to 35500. The identification of the dimer as the reactant for additional aggregation is central to the present work.

As is true for many proteins, BLG aggregation under non-denaturing conditions is most readily observed at pH close to the isoelectric point (5.2),<sup>24</sup> but a significant point for the current study is the difference between the pH of maximum aggregation and *pI*. A second point is that most reports refer to specific multimers or oligomers as opposed to open-ended aggregates. It is essential here to distinguish among multimers, oligomers, and aggregates. The first implies symmetrical structures, often biologically functional, in which differences in the intermolecular affinities of exposed and interior surfaces lead to a species not susceptible to further association. The second refers to association, often linear, in which no particular degree of association corresponds to a pronounced energy minimum. The third (the focus of the present work) may not be symmetrical, linear, or close-ended. Naturally, the consequences of intermolecular association and the particular effects of pH are concentration dependent, but even the properties of BLG gels formed at high protein concentration qualitatively show some dependence<sup>25</sup> on  $|\text{pH} - \text{pI}|$ . Depending on the pH, or salt concentration, BLG at room temperature has been reported to exist as a monomer,

a dimer, or even an octamer.<sup>26–28</sup> The monomeric form predominates below pH 3<sup>28–30</sup> and above pH 9,<sup>31</sup> but was reported to coexist in equilibrium with dimers in the pH ranges 2.0–3.7 and 5.2–9.0.<sup>32</sup> At intermediate pH values, between 3.7 and 5.2, there are reports of higher order aggregates as well,<sup>33–35</sup> with some evidence of octamer formation specifically at pH 4.7.<sup>6,29,33</sup> A number of reports conclude that aggregation increases with a decrease in ionic strength.<sup>32,36–37</sup> However, it is notable that these reports for the most part refer to close-ended association (multimerization) as opposed to the open-ended aggregation we report here.

In general, it is believed that the screening of electrostatic repulsion is a prerequisite for aggregation for all proteins, and it has been suggested that the addition of salt bridges stabilizes the BLG dimer by decreasing electrostatic repulsion between protomers at pH 3.<sup>28</sup> But electrostatic interactions can themselves enhance aggregation, as indicated by theoretical investigations.<sup>38</sup> Piazza and Iacopini<sup>35</sup> showed that attractive interactions in BLG-A solutions could lead to spontaneous formation of transient clusters. These results suggest that electrostatic interactions could play a significant role in reversible BLG aggregation. However, despite studies such as those noted above, the mechanism of BLG aggregation under non-denaturing conditions, and more specifically the role of electrostatics therein, has not been fully elucidated. Here, we examine the effects of pH and *I* on the initial aggregation rate of BLG. Two factors distinguish this work from previous studies. First, we work under non-denaturing conditions in contrast to other studies mainly concerned with heat-induced aggregation. Second, we focus on pH near *pI*, and low *I* (from 500 to 4.5 mM), which maximize electrostatic interactions. Thus, while the suppression of aggregation at high salt was noted by Piazza and co-workers,<sup>35</sup> they did not investigate ionic strengths below 200 mM<sup>35a</sup> or 50 mM,<sup>35b</sup> which, as we shall see, precludes observation of extensive aggregation at room temperature. Similarly, although Renard et al.<sup>36</sup> did examine the effects of *I* and pH, the latter was fixed at 2, 7, and 9, and consequently, only dimerization was observed.

Because of the central role of electrostatics, it is important to consider the conjoint effects of pH and ionic strength in a systematic way. Here we follow the aggregation of BLG by turbidimetry, stopped-flow spectrophotometry, and dynamic light scattering. The observations are explained using electrostatic protein modeling (Delphi); while not providing a full description of interprotein potentials, Delphi allows us to visualize the pH and *I* dependence of electrostatic potential domains around the protein and correlate those with the measured pH and *I* dependence of the initial rates. These long-range nonspecific electrostatic forces should be seen for other proteins, and recent results for the pH and ionic strength dependence of the aggregation of

(8) Surroca, Y.; Haverkamp, J.; Heck, A. J. R. *J. Chromatogr., A* **2002**, *970*, 275.

(9) Casal, H. L.; Kohler, U.; Mantsch, H. H. *Biochim. Biophys. Acta* **1988**, *957*, 11.

(10) McKenzie, H. A. *Milk Proteins* **1971**, *2*, 257.

(11) Gimel, J. C.; Durand, D.; Nicolai, T. *Macromolecules* **1994**, *27*, 583.

(12) Sawyer, W. H. *J. Dairy Sci.* **1968**, *51*, 323.

(13) Watanabe, K.; Klostermeyer, H. *J. Dairy Res.* **1976**, *43*, 411.

(14) McSwiney, M.; Singh, H.; Campanella, O. H. *Food Hydrocolloids*. **1994**, *8*, 441.

(15) McSwiney, M.; Singh, H.; Campanella, O. H.; Creamer, L. K. *J. Dairy Res.* **1994**, *61*, 221.

(16) Shimada, K.; Cheftel, J. C. *J. Agric. Food Chem.* **1989**, *37*, 161.

(17) Iametti, S.; Cairoli, S.; Gregori, De. B.; Bonomi, F. *J. Agric. Food Chem.* **1995**, *43*, 53.

(18) Surroca, Y.; Haverkamp, J. *J. Chromatogr., A* **2002**, *970*, 275.

(19) Joss, Lisa. A.; Ralston, Gregory. B. *Anal. Biochem.* **1996**, *236*, 20.

(20) McKenzie, H. A. *Adv. Protein Chem.* **1967**, *22*, 55.

(21) Green, D. W.; Aschaffenburg, R. *J. Mol. Biol.* **1959**, *1*, 54.

(22) Cecil, R.; Ogston, A. G. *Biochem. J.* **1949**, *4*, 33.

(23) Halwer, M.; Brice, B. A. *J. Colloid Sci.* **1949**, *4*, 439.

(24) Macleod, A.; Fedio, W. M.; Ozimek, L. *Milchwissenschaft* **1995**, *50*, 666.

(25) Stading, M.; Hermansson, A. M. *Food Hydrocolloids* **1990**, *4*, 121–35.

(26) Kumosinski, T. F.; Timasheff, S. N. *J. Am. Chem. Soc.* **1966**, *88*, 2635.

(27) McKenzie, H. A.; Sawyer, W. H. *Nature* **1967**, *214*, 1101.

(28) Sakurai, K.; Oobatake, M.; Goto, Y. *Protein Sci.* **2001**, *10*, 2325.

(29) Timasheff, S. N.; Townend, Robert. J. *J. Am. Chem. Soc.* **1961**, *83*, 464.

(30) Baldini, G.; Beretta, S.; Chirico, G.; Franz, H.; Maccioni, E.; Mariani, P.; Spinozzi, F. *Macromolecules* **1999**, *32*, 6128.

(31) Iametti, S.; Scaglioni, L.; Mazzini, S.; Vecchio, G.; Bonomi, F. *J. Agric. Food Chem.* **1998**, *46*, 2159.

(32) Verheul, M.; Pedersen, J. S.; Roefs, S. P. F. M.; de Kruijff, K. G. *Biopolymers* **1999**, *49*, 11.

(33) Townsend, R.; Timasheff, S. N. *J. Am. Chem. Soc.* **1960**, *82*, 3161.

(34) McKenzie, H. A.; Sawyer, W. H.; Smith, M. B. *Biochim. Biophys. Acta* **1967**, *147*, 73.

(35) (a) Piazza, R.; Iacopini, S. *Eur. Phys. J.* **2002**, *7*, 45. (b) Piazza, R.; Iacopini, S.; Galliano, *Eur. Phys. Lett.* **2002**, *59*, 149.

(36) Renard, D.; Lefebvre, J.; Griffin, M. C. A.; Griffin, W. G. *Int. J. Biol. Macromol.* **1998**, *22*, 41.

(37) Vanam, R. Thesis, Purdue University, 2004.

(38) Neves-Petersen, M. T.; Petersen, S. B. *Int. J. Biol. Macromol.* **2003**, *9*, 315.

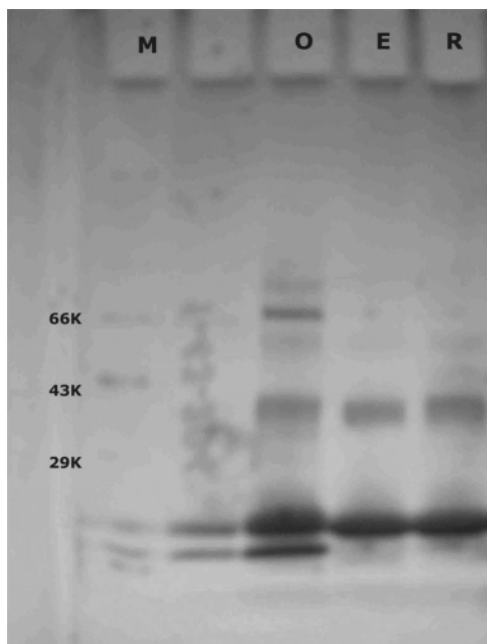


**Figure 1.** SDS-PAGE analysis of BLG: (O) lot 95H7000, (E) lot 101K7031, (R) lot 032K7035, (M) molecular weight marker [Tris-HCl Ready Gel precast gel (Bio-Rad), 4–15% linear SDS gradient, 20  $\mu$ L of 1 mg/mL BLG boiled for 1 min with 25  $\mu$ L of  $\beta$ -mercaptoethanol and 475  $\mu$ L of Laemmli buffer (75 mM Tris, 192 mM glycine, 0.1% (w/v) SDS at pH 8.3 from Bio-Rad), electrophoresed at 200 V]. The bands were visualized by silver-staining. The lowest band for lots 31 and 35 at 18 kDa is the expected BLG monomer, and the band at 36 kDa is the undissociated dimer.

insulin<sup>37</sup> demonstrate that they are both general, but at the same time a reflection of protein charge anisotropy.

## Experimental Section

**Materials.** BLG samples (A&B) (lots 95H7000, 20K7023, 101K7031, and 032K7035) were from Sigma-Aldrich, as were samples of BLG-A (lot 031K7052) and BLG-B (lot 011K7032), all subsequently referred to by the last two digits. Initial studies on the pH dependence for lot 35 were followed up with ionic strength dependence and DLS studies with lots 31 and 23. Discrepancies in the absolute rates of aggregation were noted (e.g., faster aggregation by lot 23), leading to the screening of all available lots by SDS-PAGE (see Figure 1), and the rejection of lot 95H7000 is due to the impurities such as the band near 66 kDa (possibly BSA) and another additional band of lower molecular mass than the BLG monomer. The gel scans of 31 and 35 do not show impurities, but do indicate the presence of an undissociated dimer with a molecular mass of ca. 35 kDa (about 5–10% by densitometry of the scan). The presence of this presumably disulfide linked dimer in principle might be related to variations in the absolute rates of aggregation found among these samples. We note however that the gel scan of a nondenatured chromatographically purified sample<sup>39</sup> (obtained from C. Schmitt, Nestle, Lausanne, Switzerland) also exhibited a similar ca. 36 kDa band. Thus, Sigma lots 23 and 35 with intermediate aggregation rates were used for the studies reported here because (1) the chromatographically purified BLG also displayed an initial aggregation rate (first 60 s) identical to that of lot 31 and intermediate among those of the various BLG lots, (2) the preponderance of

literature on the aggregation of BLG<sup>8,11,17,40</sup> is based on BLG from Sigma, which is presumed to not be highly denatured, and (3) most importantly, lots 20K7023, 032K035, and 101K7031 all displayed the same type of pH and ionic strength dependence of the initial aggregation rate, the central theme of this paper. This consistency also militates against the likelihood of contamination by divalent ions, leading to variable charge states and aggregation rates, as do the values of *pI* measured for several lots by electrophoretic light scattering, 4.9–5.1, all within the range of reported values.

**Sample Preparation.** BLG solutions (2 g/L) were prepared in NaCl solution at appropriate ionic strength by stirring for at least 15 min and filtering with 0.22  $\mu$ m filters (Sartorius AG, Germany) prior to use. Solutions were then adjusted to pH 9.0 to ensure formation of a stable monomer. For turbidimetric measurements a well-defined starting point (“*t*<sub>0</sub>”) was established by rapidly mixing BLG at pH 9.0, in NaCl of the desired molarity, with a solution of HCl of the same volume and ionic strength containing enough HCl to bring the pH from 9.0 to the target pH. The concentration of NaCl formed in this process is  $1 \times 10^{-5}$  M, i.e., negligible compared to the lowest ionic strength of this study,  $4.5 \times 10^{-3}$  M. The target pH was attained within about 5 s, at which point turbidimetric data were collected with a probe colorimeter (see below). Unless stated otherwise, the initial concentration of BLG at pH 9.0 was 2.0 g/L and the final concentration was 1.0 g/L. The procedure for stopped-flow spectrophotometry was essentially identical except that the target pH was attained within a few seconds.

**Methods. Turbidimetry.** Turbidity measurements were performed using a Brinkman PC 800 digital display probe colorimeter equipped with a 1 cm path length probe (420 nm), calibrated to 100% transmittance with Milli-Q water. The pH was measured with an Orion 811 pH meter equipped with a Beckman refillable combination pH electrode and calibrated with pH 7 and pH 4 buffers. The %*T* was monitored with time after the target pH was attained using the sample preparation technique described above. pH drift during the time course of the experiment was typically about 0.05 pH unit, and on the order of 0.02 pH unit or less during the time period corresponding to the initial rates. The data were reported as  $100 - \%T = \tau$  (standard deviation in  $\tau \pm 0.1\%$  transmittance unit), which is nearly linear with the true turbidity for  $100 - \%T < 10$ , an approximation entirely appropriate to our focus on the initial time dependence of  $100 - \%T$  at  $\%T > 95$ . To enhance precision, in some situations, an automatic turbidimetric titration system of our own design was used. By employing the analog signal from the colorimeter and averaging sequential readings, the standard deviation in  $\tau$  was reduced by a factor of 3 or 4.

**Stopped-Flow Spectrophotometry.** The stopped-flow experiments were performed at room temperature ( $23 \pm 1$  °C) with a Hi-Tech Scientific SF-61SX2 kintasyt stopped-flow spectrofluorimeter, equipped with a 75 W xenon lamp. All measurements were made in the absorbance mode at 420 nm. A solution of 2 g/L BLG at pH 9.0 in 0.0045 M NaCl was mixed with an equal volume of 0.0045 M NaCl solution containing the amount of acid calculated to bring the pH to a target value. The data were converted to  $100 - \%T$  before analysis.

**Dynamic Light Scattering (DLS).** DLS measurements were made after sample filtration (0.2  $\mu$ m), at a 90° scattering angle, using (1) a Brookhaven Instruments (Holtsville, NY) system equipped with a 72-channel digital correlator and an argon ion laser operating at 488 nm, with a thermostated cell (25 °C), or (2) a Malvern Instruments (Southborough, MA) Zetasizer Nanosystem ZS utilizing backscattering, with a cell temperature of 23 °C. The absence of any erratic changes in the photon count history indicated the absence of dust. The distributions of the mean apparent translational diffusion

(39) Schmitt, C.; Kolodziejczyk, E.; Lesser, M. E. In *Food Colloids: Interactions, Microstructure and Processing*; Dickinson, E., Ed.; Royal Society of Chemistry: Cambridge, 2005; Vol. 298, pp 284–300.

(40) (a) Koren, R.; Hammes, G. G. *Biochemistry* **1976**, *15*, 1165. (b) Amyard, P.; Durand, D.; Nicolai, T. *Int. J. Biol. Macromol.* **1996**, *22*, 41. (c) van Dijk, J. A. P. P.; Smit, J. A. M. *J. Chromatogr., A* **2000**, *867*, 105. (d) Schaik, H. M.; Smit, J. A. M. *Phys. Chem. Chem. Phys.* **2000**, *7*, 1537. (e) Taulier, N.; Chalikian, T. V. *J. Mol. Biol.* **2001**, *314*, 873. (f) Girard, M.; Turgeon, S. L.; Gauthier, S. F. *J. Agric. Food Chem.* **2003**, *51*, 4450. (g) Ikeda, S. *Food Hydrocolloids* **2003**, *17*, 399. (h) Kim, D. A.; Corne, M.; Narsimhan, G. *J. Colloid Interface Sci.* **2005**, *285*, 100.

coefficients ( $D_{app}$ ) were determined by fitting the DLS autocorrelation functions obtained with the Brookhaven system using CONTIN and nonnegative constrained least squares (NNLS). The reliability of the resultant multimodal distributions depends on many factors, which we have discussed at length elsewhere for systems comprising two species of distinct diffusivities<sup>41</sup> or two or three separable diffusive modes.<sup>42</sup> These analyses lead to the conclusion that distributions from the NNLS fit are more robust than those from the CONTIN fit for such complex systems. However, in the present case, the autocorrelograms are themselves time dependent; i.e., the distribution could be changing during the 1–2 min data acquisition time. Therefore, we chose to supplement data acquired with the Brookhaven system with measurements using the Malvern instrument to assess the time course of the aggregation, taking advantage of the short data acquisition times (30 s) possible with the latter instrument. The deconvolution of the autocorrelation function in this case, “Multiple Narrow Modes”, deals with signal to noise ratio (S/N) problems, which might be more severe for short acquisition times, by selection of a fixed parameter used in the minimization of residuals. In either situation, the distribution of mean apparent translational diffusion coefficients ( $D_T$ ) was converted to distributions of apparent Stokes radii via

$$R_{app} = kT/6\pi\eta D \quad (1)$$

where  $k$  is the Boltzmann constant,  $T$  is the absolute temperature, and  $\eta$  is the solvent viscosity, here assumed to be that of water.

**Computational Methods.** Computer modeling allows visualization of the electrostatic potential around the protein as a function of pH and ionic strength. In Delphi V98.0 (Molecular Simulations Inc.), the electrostatic potential around the protein is calculated by nonlinear solution of the Poisson–Boltzmann equation.<sup>43</sup> The protein crystal structures with Protein Data Bank identification 1BEB were taken from the RCSB Protein Data Bank (<http://www.rcsb.org>). However, the deposited structure 1BEB has A variant Val at position 118 and B variant Gly at position 64, which in fact corresponds neither to BLG-A (Asp64, Val118) nor to BLG-B (Gly64, Val118). To rectify this incorrect amino acid sequence, the charge file used for the electrostatic calculations was modified by replacing Gly64 with Asp64 to mimic a BLG-A dimer. The BLG-B dimer was not considered for modeling because the association of the BLG-A dimer appears to dominate aggregation effects (see below and refs 6 and 7). The amino acid charges were determined using the spherical-smear-charged model put forward by Tanford<sup>44</sup> utilizing the protein titration curve of BLG<sup>45</sup> as explained in detail elsewhere.<sup>46</sup>

## Results

**Effect of pH.** Figure 2 shows the turbidimetric time dependences for 1 g/L BLG in 0.0045 M NaCl at various initial pH values. Time zero corresponds to the time at which the target pH was attained. In the pH range 4.5–5.0, the abrupt initial increase in turbidity is followed by a stable state, but a continual increase is observed for the more extreme pH values. Our primary focus here will be on the initial apparent rate  $(d\tau/dt)_0$ , obtained as the tangent to the curve at the position of maximum slope using data collected over the first 2–3 min. This initial slope is seen in Figure 2 to attain a maximum in the vicinity of pH 4.6.

In view of the possibility of large uncertainties in  $(d\tau/dt)_0$  from turbidimetry, the results in Figure 2 were duplicated by stopped-flow spectrophotometry and the raw data (not shown) converted to 100 - %T vs time. Values of  $(d\tau/dt)_0$ , which for

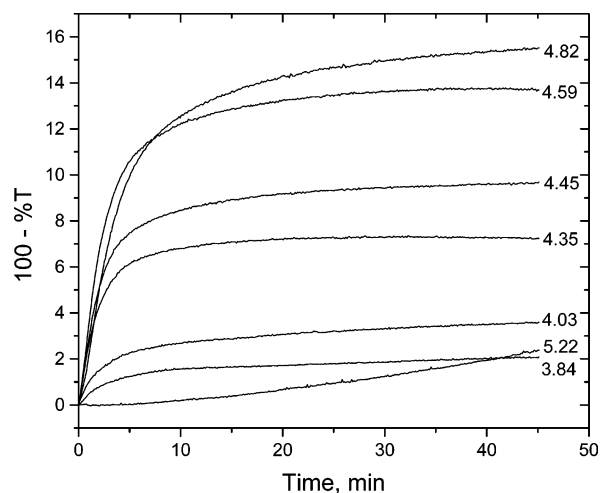


**Figure 2.** Turbidity vs time for 1 g/L BLG (lot 032K035),  $I = 0.0045$  M, at the pH values shown.

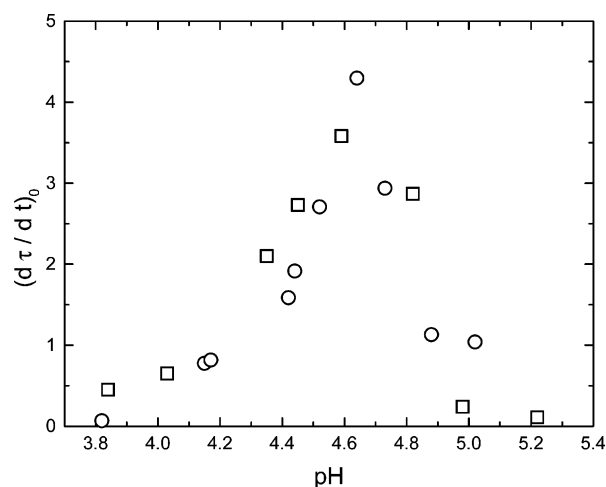


**Figure 3.** Initial rate vs pH for 1 g/L BLG (lot 032K035) at  $I = 0.0045$  M for data obtained from turbidimetry (squares) and stopped-flow spectrophotometry (circles).

stopped-flow spectrophotometry could be based on data collected as rapidly as 10 s after mixing, are shown for both techniques as a function of pH in Figure 3. The agreement between the two methods is good and indicates the excellent repeatability of the initial rate measurements. Taken together the two sets of data indicate maximum aggregation at pH 4.6–4.7 and essentially no aggregation at pH > 5.2 or < 3.8. A maximum in self-association at this pH has been noted before<sup>6</sup> but is typically referred to as a “large oligomer”, in part based on the limitations of static light scattering techniques 45 years ago, leading to the need for significant approximations in data analysis.<sup>29</sup> The large oligomer was sometimes attributed to an “octamer”, but this association is quite at odds with our observation of large turbidities and, as will be shown below, in conflict with DLS modes of very low diffusivity, both of which are consistent with open-ended association. The pH dependence of  $(d\tau/dt)_0$  is asymmetric: the effect of pH is stronger in the range 4.7–5.0 than in the range 4.3–4.6. The pH dependence of aggregation was also followed by titration of 1 g/L BLG in 10 mM NaCl from high to low pH. The results are not shown here because they are obviously dependent on the rate of titration, but the turbidity vs pH curves were found to be reversible between pH 6 and pH 4.5. Those curves displayed maxima at pH lower than 4.6, because those maxima correspond to the pH at which the rates of aggregation equal those of disaggregation. These findings, together with the

(41) Majhi, P. R.; Dubin, P. L.; Feng, X.; Guo.; Leermakers, F. A. M.; Tribet, C. *J. Phys. Chem. B* **2004**, *108*, 5980.

(42) Bohidar, H.; Dubin, P. L.; Majhi, P. R.; Tribet, C.; Jaeger, W. *Biomacromolecules* **2005**, *6*, 1573.

(43) Rocchia, W.; Alexov, E.; Honig, B. *J. Phys. Chem. B* **2001**, *105*, 6507.

(44) Tanford, C.; Kirkwood, J. G. *J. Am. Chem. Soc.* **1957**, *79*, 5333.

(45) Nozaki, Y.; Bunville, L. G.; Tanford, C. *J. Am. Chem. Soc.* **1959**, *81*, 5523.

(46) Hattori, T.; Hallberg, R.; Dubin, P. L. *Langmuir* **2000**, *16*, 9738.

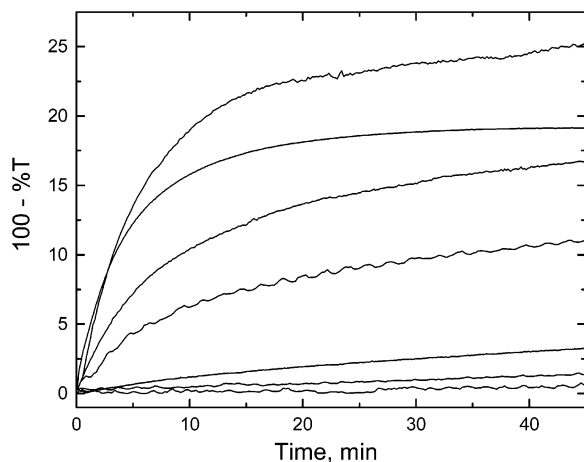


**Figure 4.** Turbidity vs time for 1 g/L BLG (lot 20K7023), pH 5.0, at different ionic strengths (from top to bottom,  $I = 0.0045, 0.006, 0.008, 0.02, 0.1, 0.3,$  and  $0.5$  M). The oscillations in the  $I = 0.02$  M curve are due to the instrument.

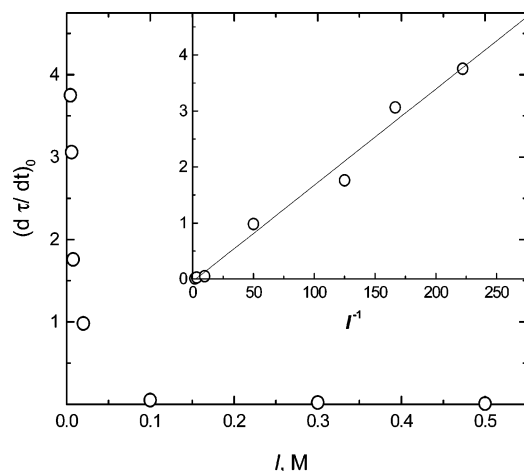


**Figure 5.** Ionic strength dependence of initial aggregation rates at pH 5.0 (from the data of Figure 4). Inset: initial rate vs  $I^{-1}$ .

reproducibility of initial rates in Figure 3, strongly indicate that the processes studied here do not involve a loss of native structure and concomitant irreversibility. Interpretation is complicated because the molecular state of the product of aggregation is unknown and may vary with time. However, light scattering studies, to be presented below, indicate that the initial reactant is mainly a dimer. While the scattering species are not readily identified, it is quite reasonable to assume that their formation, at least in the first minutes of the aggregation process, is proportional to the consumption of the reactant, which light scattering—to be presented below—clearly identifies as a dimer. The initial slope  $(d\tau/dt)_0$  is therefore considered to be proportional to the rate of dimer consumption.

**Effect of Ionic Strength.** The turbidimetric response of 1 g/L BLG at pH 5.0 for ionic strengths  $I$  ranging from 0.0045 to 0.5 M is shown in Figure 4. Significant changes in turbidity with time were not observed for  $0.1 < I < 0.5$  M. However, at  $I < 0.1$  M a sharp initial increase in turbidity was observed. Figure 5 shows the ionic strength dependence of  $(d\tau/dt)_0$ , which is seen to increase by nearly an order of magnitude with a decrease in  $I$  from 0.1 to 0.0045 M. As shown in the inset of Figure 5,  $(d\tau/dt)_0$  is linear with  $1/I$  over the entire ionic strength range. The significance of this result will be discussed later.

**Influence of A and B Variants.** Comparison of lots 23, 31, and 35 showed differences in aggregation rates at low  $I$ , with no obvious correlation to sample age, or reported purity ( $>97\%$ ).

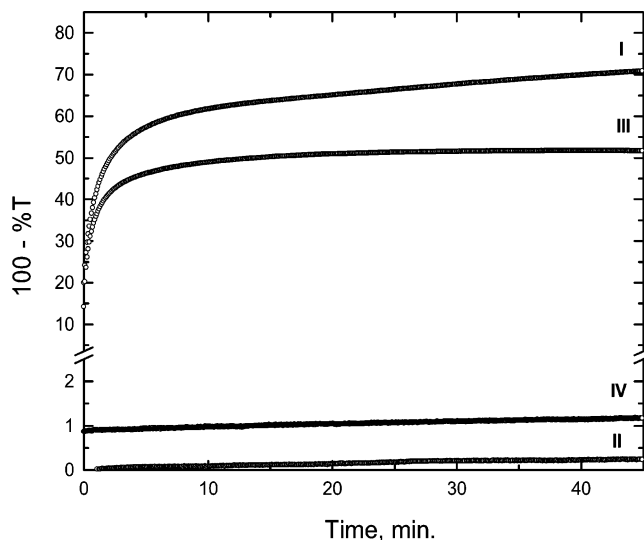


**Figure 6.** Graph showing  $100 - \%T$  vs time for BLG genetic variants A and B at  $I = 0.0045$  M: (I) 0.5 g/L BLG-A brought from pH 9.0 to pH 4.8, (II) 0.5 g/L BLG-B brought from pH 9.0 to pH 4.8, (III) 1 g/L (total concentration) BLG-A + BLG-B mixture brought from pH 9.0 to pH 4.8, (IV) 1 g/L (total concentration) BLG-A + BLG-B mixed at pH 6.0 and then brought to pH 4.8.

Although the A:B ratio was also reported to be close to 1:1 for all three lots, we decided to look into the effect of variants more closely; the results may or may not account for the differences among these lots, but are intrinsically of interest and appear to support the correlation between charge anisotropy and aggregation that is the crux of this paper.

BLG variants A and B or mixtures thereof were rapidly brought to a target pH of 4.8 (close to the pH of maximum aggregation at low salt; see Figure 2) from an initial pH of 9.0, at which all proteins are monomers. Results in Figure 6 show rapid aggregation for BLG-A (I), negligible aggregation for BLG-B (II), and intermediate aggregation when BLG-A and -B were mixed at pH 9.0 before rapid adjustment to pH 4.8 (III). However, when the pH of the A/B mixture was held at 6.0 before rapid adjustment to 4.8, negligible aggregation was observed (IV). Interpretation of these results is informed by the proposal noted above and substantiated below that the reactant at a low degree of aggregation is a dimer. In case III, AA, AB, and BB dimers could all be present, and this type of aggregation presumably occurs in all the pH and ionic strength dependence results above in Figures 2–5. The strong aggregation of the AA dimer (I) may be consistent with the results of Townsend and Timasheff,<sup>47</sup> who reported the presence of AA oligomers substantially higher than dimers. On the other hand, no aggregation is noticed with the BB dimers presumably formed in (II). This important finding points toward the sensitivity of aggregation to a small structural change. The two units of the BB dimer both lack the Asp at position 64, present in BLG-A. Reported  $pI$  values, 5.13 for BLG-A and 5.23 for BLG-B,<sup>48</sup> reflect this difference, but fail to explain its striking effect on aggregation. As will be discussed below, these two acidic amino acids lead to significantly larger negative domains in the AA dimer at pH 4.8, readily visualized by electrostatic modeling. On the other hand, the BB dimer's relatively larger positive domain at this pH can suppress its aggregation. In later discussion we will view the AA dimer, with its small but significant negative domain and its large positive domain, as an  $XY_2$  unit (X negative, Y positive) which can interact with three

(47) Townsend, Robert.; Timasheff, Serge. *N. J. Am. Chem. Soc.* **1960**, *82*, 3168.

(48) Fredriksson, S. *Anal. Biochem.* **1972**, *50*, 575.

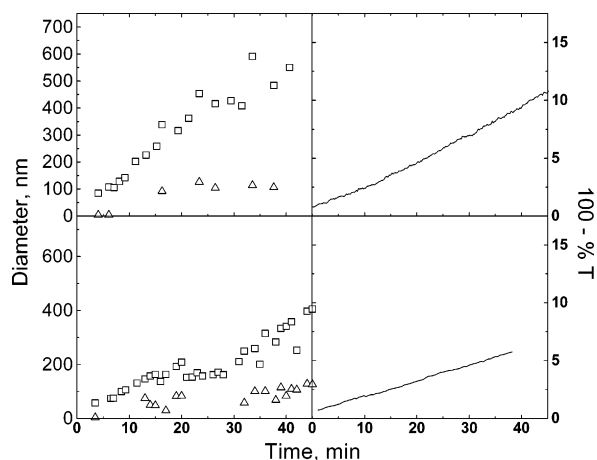


**Figure 7.** Time dependence of the apparent particle size (left) and corresponding turbidity (right) for 1 g/L BLG (lot 23) at pH 5.2 (top) and pH 5.4 (bottom), at  $I = 0.0045$  M. Symbols were used to distinguish fast ( $\Delta$ ) and slow ( $\square$ ) modes. The data are for lot 20K7023.

identical dimers. It does so by accommodating the negative (X) domains of two of the dimers in its large positive ( $Y_2$ ) domain and accommodating in its negative (X) domain a portion of the positive domain of a third AA dimer. In these terms, the BB dimer is  $Y_2$ : not only nonreactive, but also able to suppress AA self-aggregation at the proper stoichiometry. This is seen for sample IV, which contains no AB dimer, only AA and BB. These results may explain some of the lot-to-lot variability mentioned above, in that small differences in the A:B ratio could have a large effect if the BB dimer effectively suppresses the aggregation of AA, and this explanation should be considered along with the more frequent attribution of different aggregation rate variability to varying amounts of denatured material, although recent isoelectric focusing results for Sigma A/B BLG indicate no denatured material.<sup>49</sup>

**Time Dependence of the Particle Size.** To follow the aggregation process, the time dependence of the particle size was monitored by DLS. To avoid multiple scattering effects arising at high turbidities, conditions were selected corresponding to low aggregation rates, i.e., avoiding the pH range 4.3–5.1 in which aggregation is maximum. Figure 7 shows the distribution of apparent particle sizes obtained via NNLS (Brookhaven) at pH 5.2 and 5.4,  $I = 0.0045$  M, along with the corresponding turbidity curves. At both values of pH, the particle size distributions were typically bimodal with a fast mode corresponding to a diameter below ca. 100 nm and a slower mode corresponding to diameters in the range of 50–600 nm. Single values of the diameter reported for pH 5.4 (lower curve) in the range 5–15 min are artifacts arising because fast and slow modes are not adequately resolved. The turbidity is seen at both pH values to follow the growth in size of the larger particles, but bimodal distributions persist even at long times. While some scatter in the data is evident, mainly due to the need for short acquisition times, the robustness of the data and the correlation with turbidity are sufficient to convince us of the presence of a ca. 50 nm radius aggregate at 10 min and the subsequent growth of substantially larger particles. It is important to avoid overinterpretation of these values primarily because of the sensitivity of the deconvolution of the autocorrelation functions to multiple modes especially if low S/N accompanies short acquisition times. Furthermore, estimation of the number of

proteins per particle is precluded by an absence of information on the symmetry of these aggregates or their degrees of hydration.

To identify the state and presence of nonaggregated BLG, and to avoid long DLS accumulation times which would obfuscate interpretations, measurements were performed at conditions of slow association, namely, pH 4.0 and 4.2 and  $I = 0.0045$  M, utilizing the Malvern Zetasizer with which autocorrelation functions can be acquired every 30 s. The small sample volume requirement of this instrument also helped to decrease the lag time between sample preparation and measurements. Results in Figure 8 show the total scattering intensity (count rate, upper curves), the apparent diameters extracted from the autocorrelation functions (middle curves), and the absolute intensities corresponding to each mode, i.e., the fractional contribution of each mode to the total count rate (lower curves). The very short data collection times do produce more scatter, especially at low elapsed times where the total scattering is small, but certain features of the results cannot be artifactual. The data at pH 4.0, where the increase in count rate is very slow, correspond to the very early stages of aggregation and were chosen to clearly capture the signal from the 6 nm dimer, and this mode is quite evident in the data at pH 4.2 as well. The dimer, continuously present, must be very abundant in number since its scattering intensity per particle must be quite small relative to that of the larger particles. At pH 4.2 one sees the more typical faster aggregation, with the count rate leveling off after  $\sim 25$ –30 min. The higher order aggregates at pH 4.0 are confined to a ca. 300 nm diameter mode, while two distinct higher order modes of 600–700 and 200–400 nm can be identified at pH 4.2. While resolution of autocorrelation functions with significant scatter into multiple modes must be considered with caution, the entirely reasonable value for the fast mode (6 nm dimer) is noteworthy. Nevertheless, in the absence of measurements at multiple angles or of multiple algorithms to verify the size distributions, we do not speculate on the nature of species in the 200–800 nm range, but reserve our confidence to the presence of the 6 nm dimer and to the growth in size and perhaps number of considerably larger aggregates without intermediate oligomers (although such intermediates might be found under conditions of higher ionic strength). These findings are validated by the general agreement of measurements on both the BIC system (continuous open-ended association in the range of 50–500 nm at pH 5.2) and the Malvern instrument (aggregation from 100 to 500 nm at pH 4.2) despite differences in scattering angles and deconvolution algorithms. Figures 7 and 8 also indicate that the increase in scattering during the first minutes of aggregation is attributable to species with diameters of 100–200 nm, and this consistency provides some justification for the assumption that the initial time dependence of turbidity is proportional to the rate of consumption of the dimer.

## Discussion

**Reactant Is a Dimer.** The turbidity increase observed in Figures 2 and 4 could arise from many events in which the reactants could be a variety of species of different degrees of aggregation (tetramers, hexamers, etc). If this were the case, a kinetic interpretation of the change in turbidity would be difficult. However, the DLS results of Figures 7 and 8 do not show the presence of numerous intermediate species, but reveal instead at low turbidities the predominant contribution of the 6 nm diameter dimer. Accompanying the dimer are aggregates with diameters on the order of 100–800 nm. If the appearance of these aggregates is responsible for the initial increase in turbidity, then the initial slopes of Figures 2 and 4 should provide a measure

(49) Valkonen, K. H.; Martinen, N.; Malinen, H. L.; Jaakola, V. P.; Alatosava, T. *Bio-Rad Appl. Note* **1998**, 2262, 1 (also available online from Biocompare (technical article from Bio-Rad Inc.)).

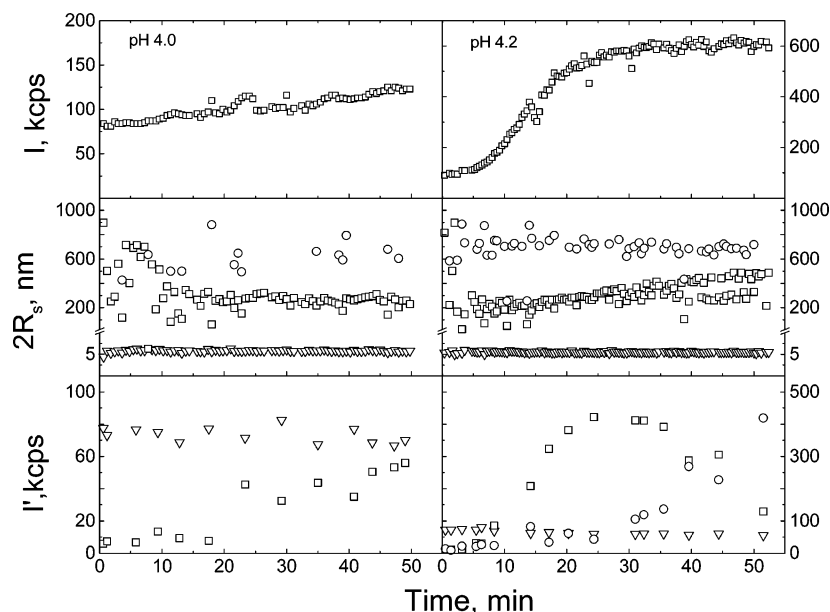


**Figure 8.** Time dependence of DLS for 1 g/L BLG (lot 20K7023),  $I = 0.0045$  M, pH 4.0 (left) and 4.2 (right): total count rate (upper), apparent diameters (middle), absolute scattering intensity corresponding to each mode (lower). Symbols in the middle and lower curves identify fast ( $\nabla$ ), slow ( $\circ$ ), and intermediate ( $\square$ ) modes, corresponding to diameters 6,  $>600$ , and 200–400 nm, respectively.

of their rates of formation. This apparent initial rate of aggregation,  $(d\tau/dt)_0$ , would be proportional to  $\tau$  if the rate of consumption of the dimer and if the scattering intensity per aggregate were constant, so the increase in  $\tau$  could be attributed to an increase in aggregate weight concentration. DLS results indicate a gradual increase in the apparent radius of the aggregate from 50 to 100 nm in the first 10–20 min, supporting the assumption of constant aggregate size during the first few minutes in which  $(d\tau/dt)_0$  is obtained. This kinetic interpretation of  $(d\tau/dt)_0$  as the rate of consumption of the dimer in a distinguishable initial process will be further justified below.

**pH Dependence of the Initial Rate.** In 0.0045 M NaCl, the initial rate of aggregation is observed to attain a maximum at pH 4.6–4.7 (less than the reported  $pI$  of BLG of 5.1–5.2<sup>50</sup>) with extreme pH sensitivity between pH 4.6 and pH 4.9. This observation, and the dramatic decrease in aggregation rate  $I > 0.02$  M, is best accounted for on the basis of electrostatic intermolecular interactions arising from protein charge heterogeneity: The asymmetry of charge and potential distributions leads to attractive forces between the positive and negative domains of associating proteins, and these local distributions are strongly influenced by the charge state of particular amino acids. As will be discussed below, this hypothesis differs from the conventional view of isoelectric precipitation. The effects proposed here are best visualized by electrostatic computer modeling, which has been used to understand similar intermacromolecular phenomena related to protein charge heterogeneity.<sup>51,52</sup> Here, protein electrostatic potential distributions for the AA dimer, chosen because of its predominant role in aggregation (see, for example, Figure 6), shown in Figure 9, help in understanding the pH and ionic strength dependence of aggregation observed in Figures 2–5. The negligibly small initial rate below pH 3.50 seen in Figure 2 is due to a large positive net protein charge, preventing association. At intermediate pH,  $(d\tau/dt)_0$  decreases 30-fold when the pH increases from 4.7 to 5.2 despite the fact that at pH = 5.2 =  $pI$ , BLG shows approximately equal positive and negative lobes (Figure 9D).

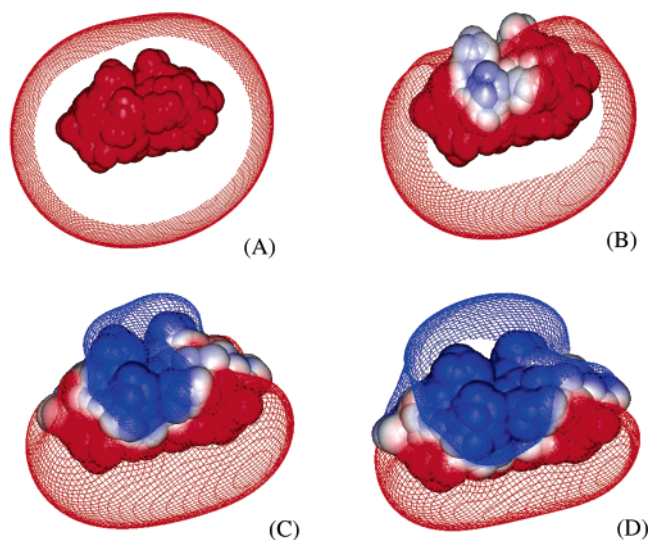


**Figure 9.** Electrostatic potential contours (+0.5 (red) and  $-0.5$  (blue)  $kT/e$ ) around the BLG dimer at ionic strength 0.0045 M, and at pH (A) 4.03, (B) 4.59, (C) 4.98, and (D) 5.22.

Many proteins exhibit diminished solubility near the isoelectric point; this phenomenon, often referred to as isoelectric precipitation,<sup>53</sup> is frequently accounted for in terms of a low protein net charge corresponding to the loss of aggregation-inhibiting repulsion. However, it is evident here from both modeling and ionic strength dependence that (a) aggregation is promoted by electrostatic attractive forces and (b) the net protein charge is not highly relevant to these forces. Thus, pH 5.2 does not correspond to conditions of maximum aggregation despite a net protein charge of zero and positive and negative lobes of similar magnitude. Maximum aggregation occurs instead at pH 4.6–4.7, where the net charge is significantly positive. While “protein solubility” is generally poorly defined, thermodynamic and rate effects often being conflated, it is quite generally reported that the “solubility” of BLG shows a minimum at pH 4.6,<sup>54,55</sup> and procedures which

(50) Righetti, Pier, G.; Caravaggio, Tiziana. *J. Chromatogr.* **1976**, *127*, 1.

(51) Seyrek, E.; Dubin, P. L.; Tribet, C.; Gamble, E. A. *Biomacromolecules* **2003**, *4*, 273.

(52) Selzer, T.; Albeck, S.; Scriber, G. *Nat. Struct. Biol.* **2000**, *7*, 537.

(53) Mathews, C. K.; van Holde, K. E.; Ahern, K. G. *Biochemistry*, 3rd ed.; Addison Wesley Longman: San Francisco, 2000.

(54) Recio, I.; Olieman, C. *Electrophoresis* **1996**, *17*, 1228.

seek to correlate the presence of denatured proteins in whey protein (primarily a mixture of BLG and  $\alpha$ -lactalbumin) advocate a pH of 4.6 for this purpose. Recognition of the contribution that might be made by native BLG to limited solubility at pH 4.6 has led to the suggestion that such tests be carried out at  $I \geq 0.1$  M.<sup>55</sup> Still, the contradiction of a maximum in isoelectric precipitation away from the isoelectric point is often overlooked.

The net charge of BLG at pH 4.6 may be significantly positive, but more importantly, the electrostatic potential contours are highly asymmetric. While we can visualize how positive and negative domains of similar size could support one-dimensional association, the ability of the large positive lobe in Figure 9B to accommodate multiple small negative domains of several other proteins suggests the multidimensional propagation that is required to account for large aggregates. While the symmetrically opposed positive and negative domains could lead to linear chains of finite length, electrostatic attraction among highly asymmetric domains could lead to branching to infinite molecular weight. This description is analogous to the difference between condensation polymerization of AB type vs condensation with AB<sub>2</sub> monomers.<sup>56</sup> From an electrostatic perspective, BLG-B dimers at pH > 4.7 might closely resemble BLG-A dimers at pH 4.7; i.e., the curves of Figure 2 might simply shift to the right. Such experiments might in the future be used to verify this analysis.

The difference between the isoionic point (5.4)<sup>45</sup> and isoelectric point (5.2) for BLG is not an uncommon observation; for BSA, for example, Tanford reported an isoionic point of 5.2, 0.3 unit above the routinely reported *pI* value of 4.9. Although it is not well understood, this observation does raise the possibility of anion binding,<sup>45</sup> particularly as the binding of chloride ion would be expected to lower the isoelectric point without a parallel change in the isoionic point. To establish whether our neglect of chloride ion binding could introduce a significant error in our modeling, we repeated calculations after removing two positive charges, corresponding to the maximum number of chloride ions bound to BLG.<sup>57</sup> No significant effect on the computed positive domain was observed. This enhances our confidence that the large positive domain at the pH of maximum aggregation is not susceptible to diminution by ion binding. For both BSA and BLG, cation binding near pH = *pI* is less significant than anion binding.

**Ionic Strength Dependence of the Initial Rate.** The dependence of the initial aggregation rate on *I* shown in Figure 5 shows  $(d\tau/dI)_0$  close to zero at  $I \geq 0.1$  M. Since the addition of salt tends to weaken electrostatic interactions, these results suggest that the suppression of aggregation at high *I* corresponds to a reduction in favorable attractive interactions due to screening effects. This behavior is also an indication that aggregation is not due to hydrophobic attraction, in which case the addition of salt would enhance aggregation and little effect would be seen at low *I*. We might also consider the effect of salt on the *pI*, since the addition of 0.15 M KCl was reported to shift *pI* from 5.4 to 5.2.<sup>45</sup> However, the effect of salt seen here is predominantly in the range of low salt.

The small variation in the electrostatic domains for ionic strengths 0.5 and 0.1 M as seen in Figure 10 accounts for the negligible differences in the initial rates at these ionic strengths. As *I* decreases below 0.1 M, the most dramatic effect is the expansion of the positive domain and the appearance of strong asymmetry between positive and negative regions with regard to both shape and magnitude. Figure 10D strengthens the

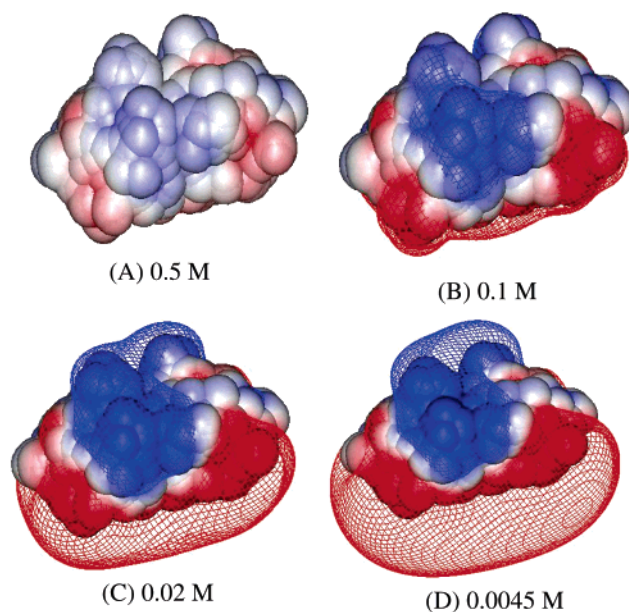


**Figure 10.** Electrostatic potential contours (+0.5 (red) and -0.5 (blue) kT/e) around the BLG dimer at pH 5 at the ionic strengths shown.

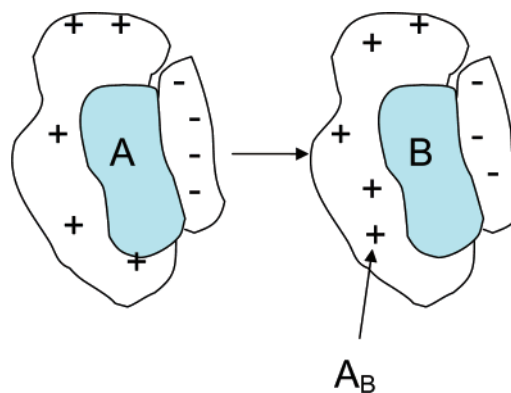


**Figure 11.** A simplified picture of protein dimer A diffusing toward protein dimer B.

hypothesis that BLG aggregates most when it has a distinct negative domain and a dominant positive domain.

The strong increase in the initial rate of aggregation with a decrease in ionic strength and the linear dependence of the initial rate on  $1/I$  can be explained by considering protein aggregation as a diffusion-controlled process. If protein A is diffusing toward protein B (both representing the dimer here) as depicted in Figure 11, the diffusion trajectory of A is given as

$$D = v_0 t \quad (2)$$

where  $v_0$  is the velocity and  $D$  is the distance a protein will travel prior to an effective encounter, requiring the corresponding time  $t$ . While it is evident that species much larger than the product of this step are formed at long times, we propose that the initial rates, especially as determined by stopped-flow spectrophotometry, relevant to the situation in which the system is essentially only a dimer, must involve as a first step collisions of dimers.

The probability that the diffusion trajectory of A intersects a cross-sectional area of B should be given by  $D$  times the cross-sectional area density of any other protein. The cross-sectional area density is obtained by multiplying the number density of the proteins,  $n/V$  ( $\text{cm}^{-3}$ ) by  $A_B$ , where  $A_B$  is the cross-sectional

(55) de Wit, J. N.; Kessel, T. V. *Food Hydrocolloids* **1969**, *10*, 143.

(56) Flory, P. J. *Principles of Polymer Chemistry*; Cornell University: Ithaca, NY, 1953; pp 376–377.

(57) Barnett, L. B.; Bull, H. B. *Arch. Biochem. Biophys.* **1960**, *88*, 328.

area (cm<sup>2</sup>) of the positive domain of B that interacts with the negative domain of A. This probability is therefore given by

$$P = D \frac{nA_B}{V} \quad (3)$$

Since the probability of effective collisions should be equal to unity, the total probability will be a dimensionless quantity equal to 1.

$$P = D \frac{nA_B}{V} = 1 = \nu_0 t \frac{nA_B}{V} \quad (4)$$

Since  $t$  here is the reciprocal of the number of encounters per unit time, the rate of the process is proportional to  $t^{-1}$ , and solving this equality for  $t^{-1}$ , assuming  $\nu_0$  and volume  $V$  are constant, reveals that the rate is directly proportional to the cross-sectional area  $A_B$ .

$$\text{rate} \propto 1/t \propto A_B \quad (5)$$

At low ionic strengths, where the Debye length ( $\kappa^{-1}$ ) is large compared to the protein radius  $R$ , the cross-sectional area  $A_B$ , which is proportional to  $(R + \kappa^{-1})^2$ , is therefore proportional to  $\kappa^{-2}$ . Since  $\kappa^{-2}$  is directly proportional to  $1/I$ , this results in a linear relationship between the initial rate of aggregation and  $1/I$ . The irregular geometry of the positive domain in Figure 10 would lead to divergence from the ideal case of a sphere, and the dependence might be in the form of  $(\kappa^{-1})^a$ , in contrast to the case of a simple sphere, where  $a = 2$ . At high ionic strengths, where charges are strongly screened and collisions in the correct orientation would be necessary, a more detailed treatment would be required. Correct orientation means that the electrostatic force must be sufficiently long range so that rapid rotation is altered as the interprotein distance falls below the Debye length. This approach is strongly validated by the efficacy of protein electrostatics in rationalizing rates of barnase–barstar complex formation as demonstrated by Schreiber and co-workers,<sup>58</sup> predicting the rate enhancement of protein complex formation from the electrostatic energy of interaction.

**Aggregation Mechanism.** DLS experiments performed at 0.6 and 0.4 pH unit above and below the maximum aggregation point (Figures 7 and 8, respectively) reveal important characteristics of BLG aggregation. The former, shown in Figure 7, displayed bimodal distributions for both pH values. For the latter case, shown in Figure 8, the presence of a distinct 6 nm mode at both pH 4.0 and pH 4.2, and its major contribution to total scattering intensity at all times for pH 4.0, and at lower times for pH 4.2, is evidence that the initial reactant of aggregation is a dimer. The absence of aggregates in the size range 10–200 nm at both of the lower pH values reveals that dimers associate to form higher order aggregates without the formation of intermediate species. These aggregates appear most prominently in the 400–600 nm range. An additional and reproducible slow mode around 700 nm was observed at pH 4.2. Its intensity begins to increase near the time at which the intensity for the 200–400 nm peak begins to decrease, so that the total count rate stabilizes.

The foregoing results suggest a two-step mechanism. The first corresponds to consumption of the dimer to form an aggregate of intermediate size whose rate of appearance thus depends on electrostatic interactions among dimers. Consequently, this process may be elucidated by protein electrostatic modeling. The second process involves a subsequent higher order association of this intermediate. As the pH approaches the pH of maximum

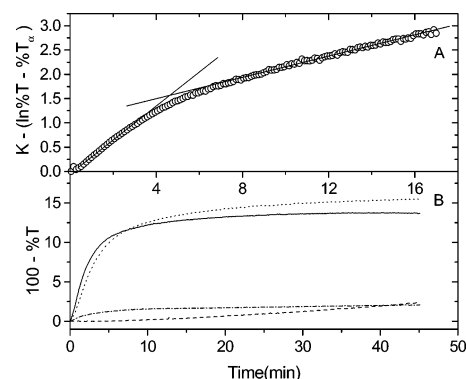


**Figure 12.** (A) Exponential fitting for aggregation data of BLG (1 g/L) at pH 4.59 and at  $I = 0.0045$  M.  $T_\infty$  is the maximum transmittance value, and  $K$  is a constant which is equal to the value of  $\ln(\%T - \%T_\infty)$  at time zero. (B) Turbidity vs time for BLG (1 g/L) at  $I = 0.0045$  M at pH values 4.82 (•••), 4.59 (—), 5.22(---), and 3.84 (-·-). The data are for lot 032K035.

initial aggregation, the time scale within which the first step can be observed decreases: it corresponds to 0–50 min for pH 4.0 and to 0–10 min for pH 4.2, after which larger aggregates appear.

To test the hypothesis of coupled and sequential aggregation steps, data obtained at pH 4.59 and  $I = 0.0045$  M are plotted semilogarithmically in Figure 12A. A single, first-order process would exhibit a linear fit with a slope proportional to the rate constant. However, the obvious deviation at  $t < 5$  min indicates the dominance of an initial mechanism with a higher rate constant. The data of Figure 12, along with the DLS results, suggest that well-defined species may exist (as opposed to a wide distribution of all possible aggregation numbers) and support a two-step process. The first step, the rapid consumption of dimers to form species on the order of ca. 200 nm (without the formation of smaller aggregates), is very sensitive to pH and corresponds to the initial turbidity slopes plotted in Figures 3 and 5. The second step, in which the 200 nm diameter intermediates form larger aggregates, is relatively slow, but can dominate the scattering. Its diminished sensitivity to pH is seen from the similarity of the slopes of the turbidity curves of Figure 12B for pH 3.84 and 4.82 after the initial rapid increase. This second step, which involves intermediate aggregates as reactants, is unlikely to be sensitive to protein charge heterogeneity, but may depend more on the net charge of a large cluster. The crossing of the curves of Figure 12 corresponding to different pH values indicates that the fast and slow steps indeed have different pH dependences.

The coexistence of dimers and large aggregates could arise from some dimers being more reactive than others, but could also be explained by analogy to the reaction of a trifunctional monomer,  $AB_2$ , in which A reacts only with B. The analogy to condensation polymerization is consistent with the gradual increase in aggregate size from 25 to 200 nm hydrodynamic radius seen in Figure 7 and consequently not in agreement with the analogy to a free radical polymerization proposed for the aggregation of heat-denatured BLG,<sup>59</sup> an entirely different case for which the charge dipoles visualized here would be clearly irrelevant. This multifunctional (branching) polymerization produces units of higher order functionality which are thus more reactive, with the very well-established result that “the rich get richer”; i.e., the system generates a mixture of high-MW species and monomers beyond the gel point,<sup>56</sup> in this case, aggregates and dimers. The appearance of a dimer even at a high degree of aggregation in this case is likely to be due to the nonreactive BB dimer (see above) rather than retroversion of the distribution.<sup>34</sup>

(58) Selzer, T.; Schreiber, G. *J. Mol. Biol.* **1999**, *287*, 409

(59) Roefs, S. P.; de Kruijff, K. G. *Eur. J. Biochem.* **1994**, *226*, 883.

This scenario explains the frequently cited observation that the increase in turbidity is maximal at a pH 0.4–0.6 pH units below the  $pI$ . Since the aggregating dimers are not at  $pI$  (net positive charge), aggregation leads to charge accumulation, and at the later stages of this process, aggregates begin to repel each other electrostatically, particularly at the low ionic strengths emphasized here. This retardation accounts for the appearance of a second kinetic regime at  $t > 4$  min in Figure 12A.

### Conclusions

The aggregation of BLG near but not at its isoelectric point is governed by electrostatic attraction between complementary charge domains among dimers. The pH dependence of the initial aggregation rate is remarkably strong and asymmetric; this is because of its sensitivity to local charges in certain electrostatic domains, which have a particularly significant role in interprotein forces. Maximum aggregation rates were observed in the pH range 4.3–4.8, below  $pI$ , where positive and negative potential domains are not of equal magnitude. The rate of aggregation strongly increased with a decrease in ionic strength  $I$  and was found to be nearly linear with  $1/I$ ; suppression of aggregation

at high ionic strengths arises from the reduction in favorable attractive interactions due to screening effects. The particle size increases with time with the appearance of bimodal distributions. The aggregation mechanism of BLG can be explained by a two-step process in which a dimer, the initial reactant, rapidly forms intermediate aggregates; these aggregates further associate, rather slowly, to form larger clusters. Since this aggregation is not at the isoionic point, the growth of aggregates may be limited by the accumulation of excess charge. Electrostatic modeling via Delphi is useful not only in elucidating the pH and ionic strength dependence of BLG aggregation but also in understanding the mechanism of aggregation.

**Acknowledgment.** Support from NSF (Grant CHE0345382) is acknowledged. Helpful suggestions were made by Dr. Michael Rubinstein and Dr. Igal Szleiffer. SDS–PAGE results were provided by Corey Trobaugh. We thank Dr. Christophe Schmitt (Nestle, Lausanne, Switzerland) for the gift of chromatographically purified BLG.

LA053528W